# Local loop opening in untangled ring polymer melts: A detailed "Feynman test" of models for the large scale structure – Supplementary Information –

Raoul D. Schram*
*Univ Lyon, ENS de Lyon, Univ Claude Bernard, CNRS, Laboratoire de Physique and Centre Blaise Pascal, F-69342 Lyon, France*

Angelo Rosa†
*SISSA - Scuola Internazionale Superiore di Studi Avanzati, Via Bonomea 265, 34136 Trieste, Italy*

Ralf Everaers‡
*Univ Lyon, ENS de Lyon, Univ Claude Bernard, CNRS, Laboratoire de Physique and Centre Blaise Pascal, F-69342 Lyon, France*
(Dated: February 12, 2019)

**Contents**



## I. MODEL RING MELT CONFORMATIONS DERIVED FROM REGULAR FRACTAL SPACE-FILLING CURVES

**Moore rings** – The Moore ring is the closed version of the Hilbert curve and both can be obtained by a recursive numerical algorithm [4]. Bead-spring Moore rings are constructed by simply arranging the monomers along the contour line of the curve. With the additional constraint of monomer density $\rho = 0.1/\sigma^3$, admissible contour lengths $Z_r$ for Moore rings occupy a cubic box of volume, $V$, given by:

$$V = \frac{6^{3/2}}{20}\, d_T^3\, Z_r\,. \tag{1}$$

$Z_r$ is thus a multiple of 8 of $Z_0 \approx \frac{64(\rho_K l_K)^{-1/2}}{L_e} \approx 5$, which leads to $Z_r = L_r/L_e = 5, 38, 307$ (see Table SI and Fig. S1).

**Hilbert ribbons** – As a hybrid between the fractal and the double-folded building strategies, we considered compact ribbon conformations where the ribbon axis follows a Hilbert curve instead of a random walk. Hilbert ribbons are built according to a procedure analogous to the construction of Klein folded rings, where now the contour length consists of a Hilbert curve. Analogously to Moore rings, Hilbert ribbons occupy a volume $V$ given by Eq. (1), where $Z_r$ is a multiple of 8 of $Z_0 \approx \frac{128(\rho_K l_K/2)^{-1/2}}{L_e} \approx 14$. This leads to $Z_r = L_r/L_e = 14, 116, 926$ (see Table SI).

Moore rings and Hilbert ribbons have been also used as starting conformations for MD computer simulations. The total number, $M$, of chains considered is summarized in Table SI.

## II. PROPERTIES OF RING MELTS CONSTRUCTED FROM DIFFERENT POLYMER MODELS: LARGE SCALE STRUCTURE

In the main text, we have focused on the ring melts derived from lattice tree melts or via hierarchical crumpling. To appreciate the success of these methods, it is useful to compare them to other plausible, but less refined models for crumpled rings, which we have studied in Ref. [3]. Below, we provide more details and analyze the same observables ($\langle R^2(L)\rangle, C_N(L), p_c(L), \Omega(L)$) as in the main text.

**Klein ribbons** – For a ribbon axis with the same Kuhn length as in the fiber model, the conformational statistics of tightly wrapped rings turns out to be in almost perfect agreement with the corresponding Gaussian rings [3]: in particular, the mean-square internal distances obtained for the constructed Klein ribbons (dotted lines in Fig. S2a) are equivalent to the Gaussian ring law, $\langle R^2(L)\rangle = l_K L\left(1 - \frac{L}{L_r}\right)$, where the average is taken over all monomers of a ribbon with vanishing diameter and an axis with the same stiffness / Kuhn length as the chains. As a consequence, there is also perfect agree-

*Electronic address: raoul.schram@ens-lyon.fr
†Electronic address: anrosa@sissa.it
‡Electronic address: ralf.everaers@ens-lyon.fr

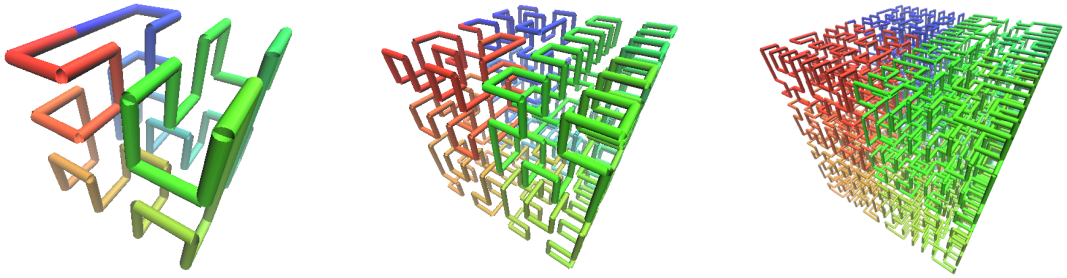

Fig. S 1: Moore curves. From left to right are shown the first ($Z_r = 4.8$), second ($Z_r = 38.4$) and third ($Z_r = 307.2$) generation of a single ring polymer.

| Initial state | $Z_r$ | $N \times M \times$ #RUNS | $\tau_{tot}[\tau_{LJ}]$ | $\tau_{tot}/\tau_{eq}$ |
|---|---|---|---|---|
| Klein ribbon (I) | 4.8 | $190 \times 1 \times 1^*$ | $1.2 \times 10^7$ | $2 \times 10^3$ |
| Klein ribbon (II) | 4.8 | $194 \times 1 \times (\gtrsim 100)^*$ | $1.2 \times 10^7$ | $2 \times 10^3$ |
| Moore ring | 4.8 | $192 \times 8 \times 1$ | $1.2 \times 10^8$ | $2 \times 10^4$ |
| Ideal LT ribbon | 5.0 | $200 \times 32 \times 1$ | $1.2 \times 10^7$ | $2 \times 10^3$ |
| Klein ribbon (I) | 14.7 | $589 \times 1 \times 1^*$ | $1.2 \times 10^8$ | $1.5 \times 10^3$ |
| Klein ribbon (II) | 14.5 | $582 \times 1 \times (\gtrsim 100)^*$ | $1.2 \times 10^7$ | $1.5 \times 10^2$ |
| Hilbert ribbon | 14.3 | $570 \times 8 \times 1$ | $1.2 \times 10^8$ | $1.5 \times 10^3$ |
| Ideal LT ribbon | 15.0 | $600 \times 8 \times 1$ | $1.2 \times 10^8$ | $1.5 \times 10^3$ |
| Klein ribbon (I) | 34.7 | $1388 \times 1 \times 1^*$ | $1.2 \times 10^8$ | $1 \times 10^2$ |
| Klein ribbon (II) | 34.9 | $1396 \times 1 \times (\gtrsim 100)^*$ | $1.2 \times 10^7$ | $1 \times 10^1$ |
| Moore ring | 38.4 | $1536 \times 8 \times 1$ | $2.4 \times 10^8$ | $2 \times 10^2$ |
| Ideal LT ribbon | 37.6 | $1502 \times 16 \times 1$ | $1.2 \times 10^8$ | $1 \times 10^2$ |
| Klein ribbon (I) | 110.8 | $4433 \times 1 \times 1^*$ | $1.2 \times 10^9$ | $\mathcal{O}(10)$ |
| Klein ribbon (II) | 110.2 | $4409 \times 1 \times (\gtrsim 100)^*$ | $1.2 \times 10^7$ | $\mathcal{O}(0.1)$ |
| Hilbert ribbon | 115.5 | $4620 \times 8 \times 1$ | $6.0 \times 10^8$ | $\mathcal{O}(5)$ |
| Ideal LT ribbon | 115.1 | $4605 \times 8 \times 1$ | $1.2 \times 10^8$ | $\mathcal{O}(1)$ |
| Moore ring | 307.2 | $12288 \times 8 \times 1$ | $1.2 \times 10^8$ | – |
| Hilbert ribbon | 925.6 | $37024 \times 1 \times 1$ | $1.2 \times 10^8$ | – |

Table S I: Details of the ring systems studied by Molecular Dynamics computer simulations (Sec. IIA in the main text). Initial states correspond to (a) the lattice models described in Sec. IID in the main text and (b) the fractal models described in Sec. I here. $Z_r$: number of entanglements per single ring; $N$: number of Lennard-Jones monomers per single ring; $M$: number of rings per each system; #RUNS: total number of independent MD runs; $\tau_{tot}$: time-length of the single MD trajectory, expressed in elementary Lennard-Jones (LJ) [1, 2] time steps ($\tau_{LJ}$); $\tau_{tot}/\tau_{eq}$: total number of independent MD configurations, where $\tau_{eq}$ is the *diffusion* equilibration time corresponding to chain motion beyond the polymer mean gyration radius. *There are two sets of MD simulations for Klein ribbons. Set I includes data from Ref. [3] and is used for Figs. 2, 4 and 5 in the main text and Figs. S2 and S6 here. Set II includes data consisting of, at least, #RUNS independent simulations of one-ring systems and is used for Fig. S8 here.

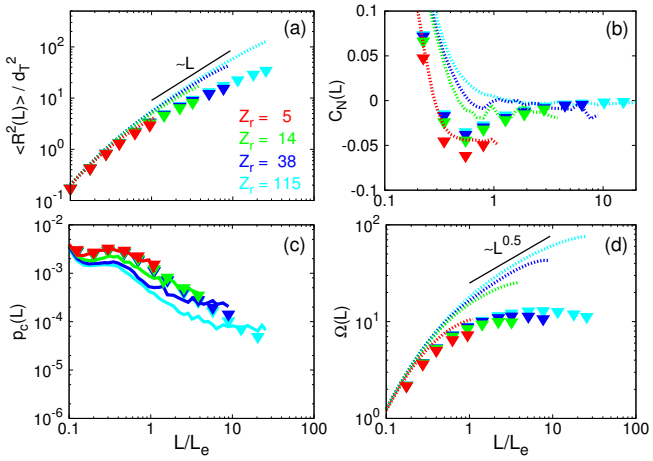


Fig. S 2: Comparison of the conformational statistics for MD-equilibrated rings (symbols) and Klein ribbons (lines: dotted, average at $t = 0$; solid, average at $t = \tau_e$). (a) $\langle R^2(L)\rangle$, Mean-square internal distances. (b) $C_N(L)$: Bond-vector orientation correlation function. (c) $p_c(L)$: Mean contact probability between monomers for contact distance $\leq 2\sigma$. (d) $\Omega(L)$: Overlap parameter. Data extend up to 1/4 of the corresponding rings contour lengths. The same observables are used in Fig. 3 in the main text and Figs. S3-S5.

ment for quantities which can be derived from $\langle R^2(L)\rangle$ such as the gyration radius [3], or the bond-vector orientation correlation function, Eq. (4) in the main text, which decays on the Kuhn scale and drops to $-l_K/L$ for large distances as a consequence of the closure constraint (Fig. S2b). The difference between the random walk ribbons and Gaussian rings only becomes apparent from the asymmetry ratios of the gyration tensor [3]: by construction, for large Klein ribbons we find the typical values for ordinary random walks $\approx 11.7 : 2.7 : 1.0$ [5], at odds with the measured $\approx 6.1 : 2.3 : 1.0$ for Gaussian rings [6].

By construction, the linear ribbon model predicts the $L^{1/2}$ growth of the overlap parameter, $\Omega(L) \equiv \frac{\rho_K l_K}{L}\langle R^2(L)\rangle^{3/2}$, which is characteristic for linear chains (Fig. S2d). For ring sizes up to a few entanglement lengths, long (up to $\approx 10^6\tau_e$, see Table SI) MD equilibration runs of Klein folded initial states hardly affect the conformational statistics. However, larger rings undergo substantial shrinking (Fig. S2a) with correspondingly increased contact probabilities (Fig. S2c), develop anti-correlations in the bond-vector orientation correlation

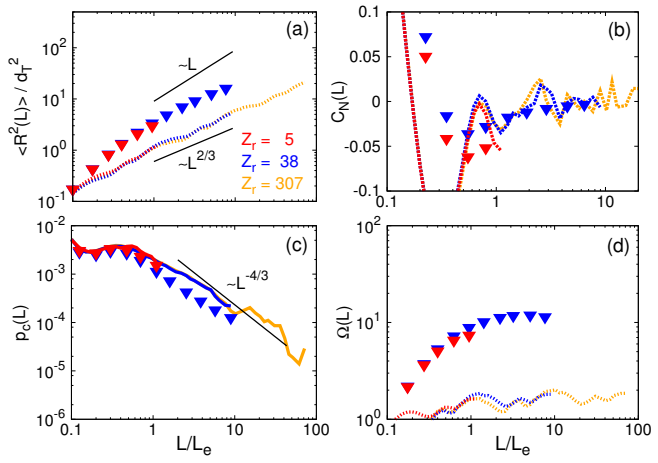


Fig. S 3: Comparison of the conformational statistics for MD-equilibrated rings (symbols) and space-filling Moore rings (lines: dotted, average at $t = 0$; dashed, average at $t = 0.1\tau_e$; solid, average at $t = \tau_e$).

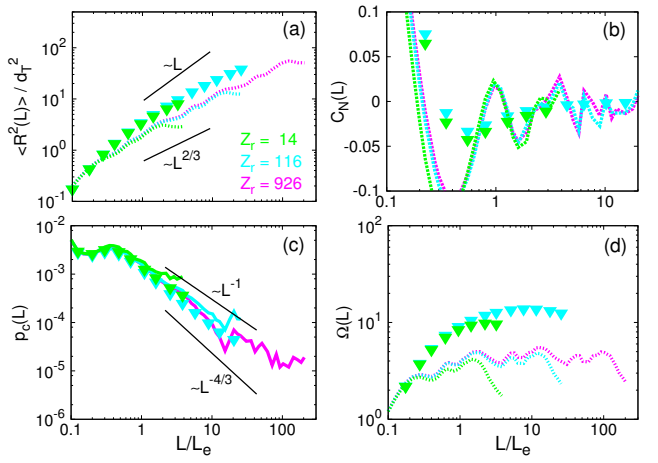


Fig. S 4: Comparison of the conformational statistics for MD-equilibrated rings (symbols) and space-filling Hilbert ribbons (lines: dotted, average at $t = 0$; dashed, average at $t = 0.1\tau_e$; solid, average at $t = \tau_e$).

function on the entanglement scale (Fig. S2b), and lower the overlap parameter (symbols in Fig. S2d) slightly below the entanglement threshold, $\Omega \equiv 20$ [7–9].

**Moore rings** – In melts derived from standard space-filling curves neighboring rings do not overlap at all. The lines in Fig. S3 represent the conformational properties of Moore rings. Panel (a) and panel (c) (whose curves were averaged after a short MD run up to $\tau_e$) show that $\langle R^2(L)\rangle \sim L^{2/3}$ and $p_c(L) \sim L^{-4/3}$ in agreement with [10]. The regular structure manifests itself in an oscillating bond-vector orientation correlation function (Fig. S3b, curves averaged after a short MD run up to $\tau_e/10$, sufficient to equilibrate the chain statistics below the entanglement scale). Interestingly, the overlap parameter of $\approx 2$ [11] never approaches the entanglement threshold of $\Omega = 20$ (Fig. S3d).

We have also performed long (up to $\approx 10^5\tau_e$, see Table SI) MD simulations to equilibrate systems with $Z_r = 5$ and $Z_r = 38$ (symbols in Fig. S3). In our final conformations the oscillations in the bonds orientations are again replaced by anti-correlations on the entanglement scale. In particular, the Moore conformations undergo substantial swelling, increasing the overlap parameter on large length scales close to the entanglement threshold. We remark, that the relaxation of the scaling exponent for contact probabilities $p_c(L)$ which *increases* from $\approx -4/3$ to $\approx -1$ (Fig. S3c) is another signature of the important difference between (a) polymer confinement in the presence of surrounding chains which forces the ring to branch and assume rugged surfaces and (b) polymer confinement inside smooth environments which was originally [10] indicated as a possible recipe to assemble crumpled globules: as later demonstrated in [12], the latter strategy fails producing stable polymer conformations as the scaling exponent is found *to decrease* from $\approx -4/3$ to $\approx -1.5$, *i.e.* close to the value expected for an equilibrium globule.

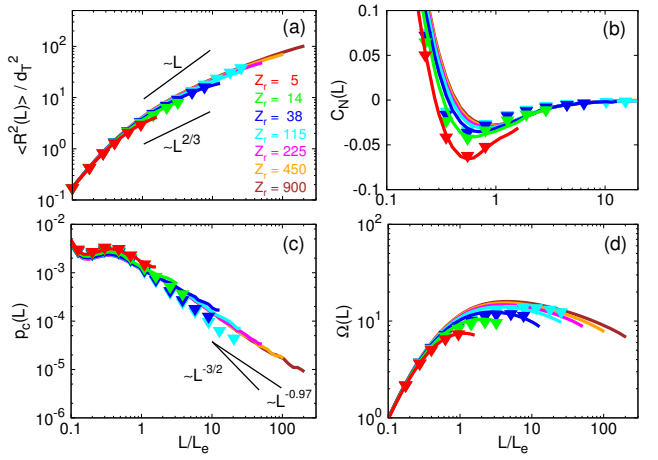


Fig. S 5: Comparison of the conformational statistics for MD-equilibrated rings (symbols) and ideal lattice tree ribbons (solid lines, average at $t = \tau_e$). Notice, that the large-scale decay of contact probabilities, $p_c(L) \sim L^{-0.97\pm0.01}$ (panel (c)), is different from the observed behavior of rings obtained from the interacting lattice tree model (see panel (c1) of Fig. 3 in the main text). Note also the slow divergence of the overlap parameter with chain length (panel (d)).

**Hilbert ribbons** – The Hilbert ribbons have a similar conformational statistics as Moore rings (Fig. S4). The typical size grows like $\langle R^2(L)\rangle \sim L^{2/3}$ as long as $L \ll L_r$. The conformations are locally less crumpled. The overlap parameter (Fig. S4d) of $\approx 5$ is nearly twice as large as for Moore rings [13], but it stays nevertheless well below the entanglement threshold. Interestingly, contact probabilities decay like $p_c(L) \sim L^{-1}$ (Fig. S4c) in better agreement with the experimental [10] and simulation data [14]. For $Z_r = 14$ and $Z_r = 116$ we have prepared

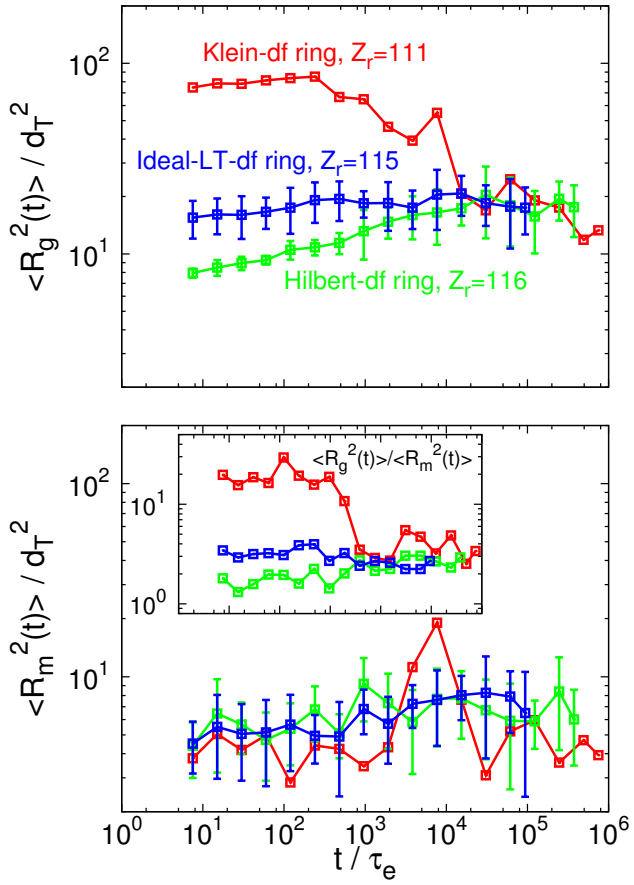


Fig. S 6: Time behaviors of the average square gyration radius ($\langle R_g^2(t)\rangle$, top) and the average square magnetic radius ($\langle R_m^2(t)\rangle$, bottom) for solutions of ring polymers with different initial conformations: (1) Klein double-folded rings (red), (2) Hilbert double-folded rings (green) and (3) double-folded rings on ideal branched primitive paths (blue). Systems (2) and (3) are made of 8 rings, while system (1) is made of only one chain. The inset shows the ratio $\langle R_g^2(t)\rangle/\langle R_m^2(t)\rangle$. Error bars are for the standard deviation of the mean.

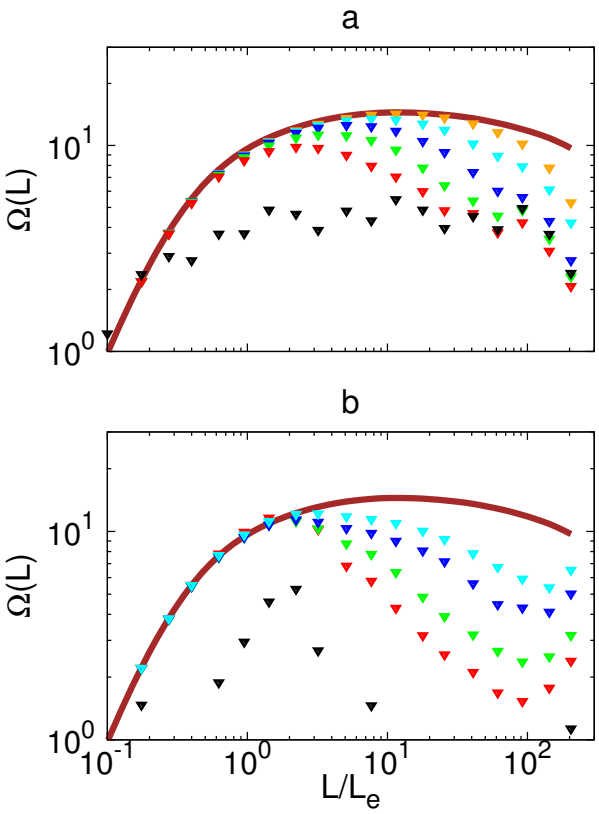


Fig. S 7: MD-equilibration of overlap parameter, $\Omega(L)$, shows the clear progression from small to large contour-length separations. Symbols of different colors correspond to square internal distances averaged over exponentially larger and larger time windows: black symbols show data corresponding to the initial configuration; symbols from red to orange represent MD data averaged over $10^i < t/\tau_e < 10^{i+1}$, with $i$ from 0 to 4 respectively (there are no data for $i = 4$ in panel (b)). The two panels show: (a) the largest ($Z_r = 926$) Hilbert ribbon (see Table SI here), (b) the linear polymer chains the size the human chromosomes ($Z = 810$) studied in [15]. The brown solid line is the prediction of the interacting lattice tree model.

(see Table SI) equilibrated melt conformations starting from $M = 8$ chains with identical Hilbert ribbon conformations (symbols in Fig. S4). Again, the oscillations in the bonds orientations are replaced by anti-correlations on the entanglement scale with the rings swelling close to the entanglement threshold.

**Branched ribbon conformations from the *ideal* lattice tree model** – Results for rings derived from melts of ideal lattice trees are illustrated in Fig. S5 (solid lines). We note the characteristic anti-correlations of bonds orientations (panel (b)) on the entanglement scale and the overlap parameter just below the entanglement threshold (panel (d)). Again, we have constructed topologically correct melt states by assembling single ring conformations at the correct monomer density into a simulation box with periodic boundary conditions. Starting from these, we have run MD simulations for as long as in the previous cases (*i.e.* $\approx 10^5\tau_e$, see Table SI). Results for MD simulations are summarized as symbols in Fig. S5. We notice that, while small rings (up to $Z_r = 38$, blue symbols) are well described by the ideal lattice tree model, the cyan system ($Z_r = 115$) starts showing some swelling, especially evident in the overlap parameter (panel (d)).

## III. BRUTE-FORCE MOLECULAR DYNAMICS (MD) EQUILIBRATION OF "GOLD STANDARD" REFERENCE DATA

Table SI lists the specifications of the ring melts, which we have studied [3] using Molecular Dynamics simula-

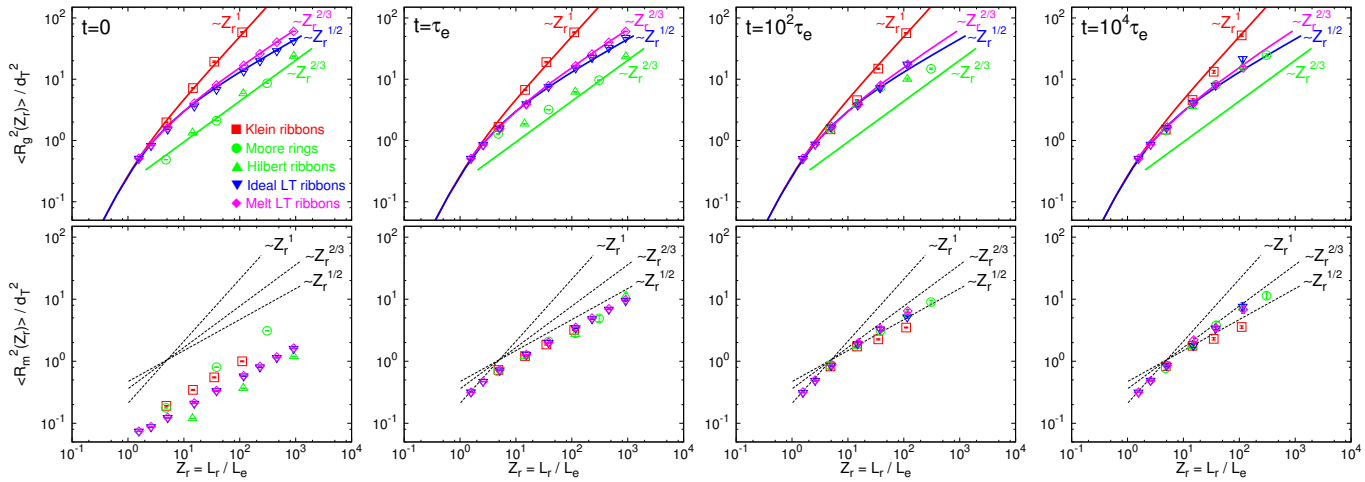


Fig. S 8: Equilibration of gyration (top row) and magnetic (bottom row) radii in Molecular Dynamics simulations of the fiber model. Lines with different colors correspond to the theoretically expected gyration radii for the different types of structures. Symbols refer to simulation data for ensembles derived from corresponding initial states. Not all systems were run to the maximal time (see Table SI here), explaining the different number of symbols used in the different panels.

tions.

Fig. S6 illustrates the time evolution for the average gyration and magnetic radii ($\langle R_g^2(t)\rangle$ and $\langle R_m^2(t)\rangle$, top and bottom panel respectively) for our largest ring polymers with $Z_r \approx 100$ and different initial conformations (see Sec. IID in the main text, Sec. I here and Table SI). As expected, after a long transient the memory of the initial conformation is lost and both observables fluctuate around their corresponding equilibrium values with ratio $\langle R_g^2(t)\rangle/\langle R_m^2(t)\rangle \approx 2.1$ (see inset of bottom panel). As in the case of relaxation of long, untangled linear chains [15], rings equilibration proceeds from small to large scales (Fig. S7). As illustrated by Fig. S8, the magnetic and the gyration radius equilibrate on similar time scales. In particular, this implies that the lattice tree melt derived ring melts are *not* equilibrated and would need to be brute-force equilibrated like any other topologically correct initial state.


[1] S. Plimpton, J. Comp. Phys. **117**, 1 (1995).

[2] K. Kremer and G. S. Grest, J. Chem. Phys. **92**, 5057 (1990).

[3] A. Rosa and R. Everaers, Phys. Rev. Lett. **112**, 118302 (2014).

[4] H. Sagan, *Space-Filling Curves* (Springer, New York, NY, 1994).

[5] J. Rudnick and G. Gaspari, Science **237**, 384 (1987).

[6] M. Bishop and J. P. J. Michels, J. Chem. Phys. **82**, 1059 (1985).

[7] T. A. Kavassalis and J. Noolandi, Phys. Rev. Lett. **59**, 2674 (1987).

[8] L. J. Fetters, D. J. Lohse, D. Richter, T. A. Witten, and A. Zirkel, Macromolecules **27**, 4639 (1994).

[9] N. Uchida, G. S. Grest, and R. Everaers, J. Chem. Phys. **128**, 044902 (2008).

[10] E. Lieberman-Aiden et al., Science **326**, 289 (2009).

[11] This is not an artifact of the particular form of the Moore curve, but a consequence of the more general construction principle of filling space by subsequently occupying neighboring cubic blocks. Let $a$ denote the linear dimension of such a block, which contains a chain contour length of $L(a)$. By construction, there is only a single chain of length $L(a)$ contained in the volume $a^3$, so that the contour length density is $\rho_{cl} = L(a)/a^3$. If the path enters the block at one corner and exits through a neighboring corner at a distance $\langle R^2(L(a))\rangle = a^2$, across a face diagonal at a distance $\langle R^2(L(a))\rangle = 2a^2$, or across a body diagonal at a distance $\langle R^2(L(a))\rangle = 3a^2$, then the overlap parameter on this length scale is given by $1^{3/2} = 1$, $2^{3/2} \approx 2.8$, and $3^{3/2} \approx 5.2$ respectively.

[12] R. D. Schram, G. T. Barkema, and H. Schiessel, J. Chem. Phys. **138**, 224901 (2013).

[13] It is easy to show that the overlap parameters between Moore rings and Hilbert ribbons differ by a factor of $\approx 2$, and that similar relations should hold for other space-fillings curves which are constructed by subsequently occupying neighboring cubic blocks. Let $a$ denote the linear dimension of such a block, which contains a chain contour length of $L(a)$ [11]. For analogs of the Hilbert ribbons the contour length density is $\rho_{cl} = 2\,L(a)/a^3$, since the volume contains two independent chain sections. As a consequence, the overlap parameter increases by a factor of two.

[14] A. Rosa, N. B. Becker, and R. Everaers, Biophys. J. **98**, 2410 (2010).

[15] A. Rosa and R. Everaers, Plos Comput. Biol. **4**, e1000153 (2008).